Pliocene–Pleistocene basin evolution along the Garlock fault zone, Pilot Knob Valley, California

William M. Rittase[1],*, J. Douglas Walker[1], Joe Andrew[1], Eric Kirby[2], and Elmira Wan[3]

[1]Department of Geology, University of Kansas, Lawrence, Kansas 66045, USA
[2]College of Earth, Ocean and Atmospheric Sciences, Oregon State University, Corvallis, Oregon 97330, USA
[3]U.S. Geological Survey, 345 Middlefield Road, Menlo Park, California 94025, USA

ABSTRACT

Exposed Pliocene–Pleistocene terrestrial strata provide an archive of the spatial and temporal development of a basin astride the sinistral Garlock fault in California. In the southern Slate Range and Pilot Knob Valley, an ~2000-m-thick package of Late Cenozoic strata has been uplifted and tilted to the northeast. We name this succession the formation of Pilot Knob Valley and provide new chronologic, stratigraphic, and provenance data for these rocks. The unit is divided into five members that record different source areas and depositional patterns: (1) the lowest exposed strata are conglomeratic rocks derived from Miocene Eagle Crags volcanic field to the south and east across the Garlock fault; (2) the second member consists mostly of fine-grained rocks with coarser material derived from both southern and northern sources; and (3) the upper three members are primarily coarse-grained conglomerates and sandstones derived from the adjacent Slate Range to the north. Tephrochronologic data from four ash samples bracket deposition of the second member to 3.6–3.3 Ma and the fourth member to between 1.1 and 0.6 Ma. A fifth tephrochronologic sample from rocks south of the Garlock fault near Christmas Canyon brackets deposition of a possible equivalent to the second member of the formation of Pilot Knob Valley at ca. 3.1 Ma. Although the age of the base of the lowest member is not directly dated, regional stratigraphic and tectonic associations suggest that the basin started forming ca. 4–5 Ma. By ca. 3.6 Ma, the northward progradation fanglomerate sourced in the Eagle Crags region waned, and subsequent deposition occurred in shallow lacustrine systems. At ca. 3.3 Ma, southward progradation of conglomerates derived from the Slate Range began. Circa 1.1 Ma, continued southward progradation of fanglomerate with Slate Range sources is characterized by a shift to coarser grain sizes, interpreted to reflect uplift of the Slate Range. Overall, basin architecture and the temporal evolution of different source regions were controlled by activity on three regionally important faults—the Garlock, the Marine Gate, and the Searles Valley faults. The timing and style of motions on these faults appear to be directly linked to patterns of basin development.

■ INTRODUCTION

Pilot Knob Valley is a 45 km × 6 km, east-west–elongated depression located south of the Slate Range, in eastern California (Fig. 1). The active strand of the central Garlock fault cuts ENE-WSW across the northern third of the valley, and a sequence of Pliocene to Pleistocene deposits are deformed and exposed between the active trace of the Garlock and the Slate Range to the north. Basin deformation and inversion are Pleistocene–Holocene in age and provide the opportunity to study earlier sedimentation patterns along the Garlock fault zone. Faults active during deposition of these rocks include the sinistral Garlock fault, a secondary Garlock fault strand named the Marine Gate fault (Andrew et al., 2014a), and the low-angle normal slip Searles Valley fault to the north in Searles Valley (Walker et al., 2005; Numelin et al., 2007).

J. Douglas Walker https://orcid.org/0000-0002-3706-2729
*Now at Concho Resources, Midland, Texas 79701, USA

In this contribution, we present a refined stratigraphy of uplifted Pliocene to Pleistocene sedimentary rocks along the Garlock fault, evaluate changes in the provenance of sediments through time, and place age constraints on sedimentation and changes in basin development. All strata represent terrestrial facies associated with alluvial fans and playa basins. In this paper, we describe these strata in detail and interpret the evolution of their depositional environments and basin development through time.

■ GEOLOGIC SETTING

This section describes the faults active during basin development and features of the geology of surrounding areas critical to understanding sediment provenance. The study area is in the zone of complex faulting called the Eastern California shear zone or Walker Lane belt. This is a north-northwest–trending nest of dextral transcurrent and transtensional faults. The zone is similar to the San Andreas fault but smaller in slip rate (~1/3 of that on the San Andreas) (Miller et al., 2001) and total slip. This deformation began at ca. 4 Ma (Andrew and Walker, 2017). This zone is crossed by the sinistral Garlock fault that started motion at ca. 12 Ma (Andrew et al., 2015). It is along this latter fault that the Pilot Knob Valley develops. Acceleration of motion along the Garlock began when the Walker Lane became active. Our descriptions and interpretations below address how the sinistral Garlock fault interacts with the dextral zone. The work reported here for the provenance of clasts records the changes in sediment sources from both the north and south of the Garlock fault over the
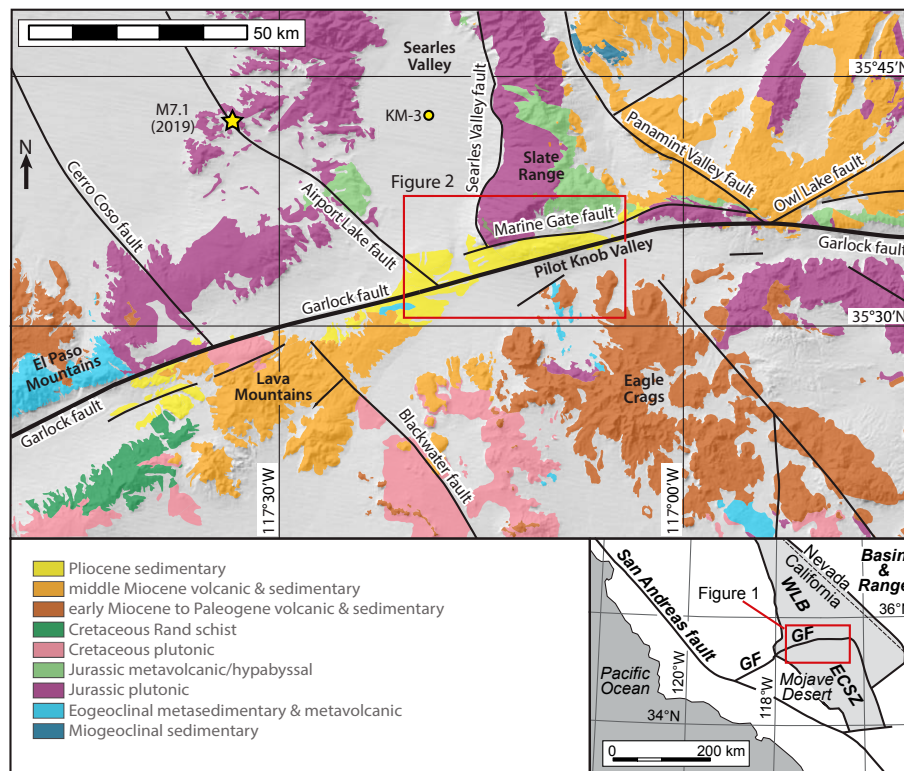
Figure 1. Location map of the study area in reference to the eastern California shear zone (inset map) with regional geology of the study area showing the location of our detailed studies as red box. Figure constructed using a U.S. Geological Survey base map at https://basemap.nationalmap.gov/arcgis/rest/services/USGSShadedReliefOnly /MapServer. WLB—Walker Lane Belt; GF—Garlock fault; ECSZ—eastern California shear zone.

2015). The sedimentary rocks discussed in this paper are sandwiched between these major structures. These two faults form the Garlock fault zone, which has ~60 km of net slip in this area (Andrew et al., 2015). The Garlock fault is the main, through-going strike-slip fault in the area. The Marine Gate fault is currently active as a north-side-up, high-angle fault. However, it appears to have accommodated ~20 km of sinistral motion during late Miocene to Pleistocene times (Andrew et al., 2015). The Marine Gate fault is also well imaged in the subsurface, bounding the south side of a basin up to 3 km thick (Monastero et al., 2002). Andrew et al. (2015) described a detailed slip history for the Garlock fault zone in this region. Two NNW-striking dextral strike-slip faults also occur in the nearby region: the Airport Lake and Panamint Valley and Brown Mountain faults (Figs. 1 and 2). Each fault has several kilometers of slip (Andrew and Walker, 2009; Walker and Andrew, 2019; Walker et al., 2019).

Normal Faults

The western boundary of the Slate Range is formed by the Searles Valley fault (Walker et al., 2005; Numelin et al., 2007), a low-angle normal fault with inferred motion initiating at ca. 4 Ma (Walker et al., 2014). This down-to-the-west fault appears to be integrated northward with the Panamint Valley and Ash Hill faults (Walker et al., 2005; Andrew and Walker, 2009). Field mapping by Rittase (2012) suggests a southern termination against the Marine Gate fault in Pilot Knob Valley. On the east side of the Slate Range, the Panamint Valley fault has mostly dextral motion near the Garlock fault (Zhang et al., 1990) but is a normal dextral-oblique fault northward with down-to-the-west slip (Walker et al., 2005).

Geology of the Potential Clast Source Uplands

Distinct rock types in the ranges surrounding Pilot Knob Valley help establish clast provenance

past ~5 m.y. Sources and changes in source areas are essential to unraveling the slip history of the Garlock fault (Andrew et al., 2015). The descriptions in this paper rely on recent geologic maps of the southern Slate Range and Pilot Knob Valley (Andrew et al., 2014a) and the Lava Mountains (Andrew et al., 2014b).

Major Faults

Several major faults transect the study area and appear to have controlled basin development and

inversion. These faults created accommodation space for the basin, uplifted the various distinctive source regions for sediment provenance, and laterally displaced the basin strata away from source regions.

Strike-Slip Faults

The most prominent faults in the area are WSW-striking sinistral strike-slip faults, the Garlock fault, and the newly identified Marine Gate fault (Fig. 2; Rittase, 2012; Andrew et al., 2014a,
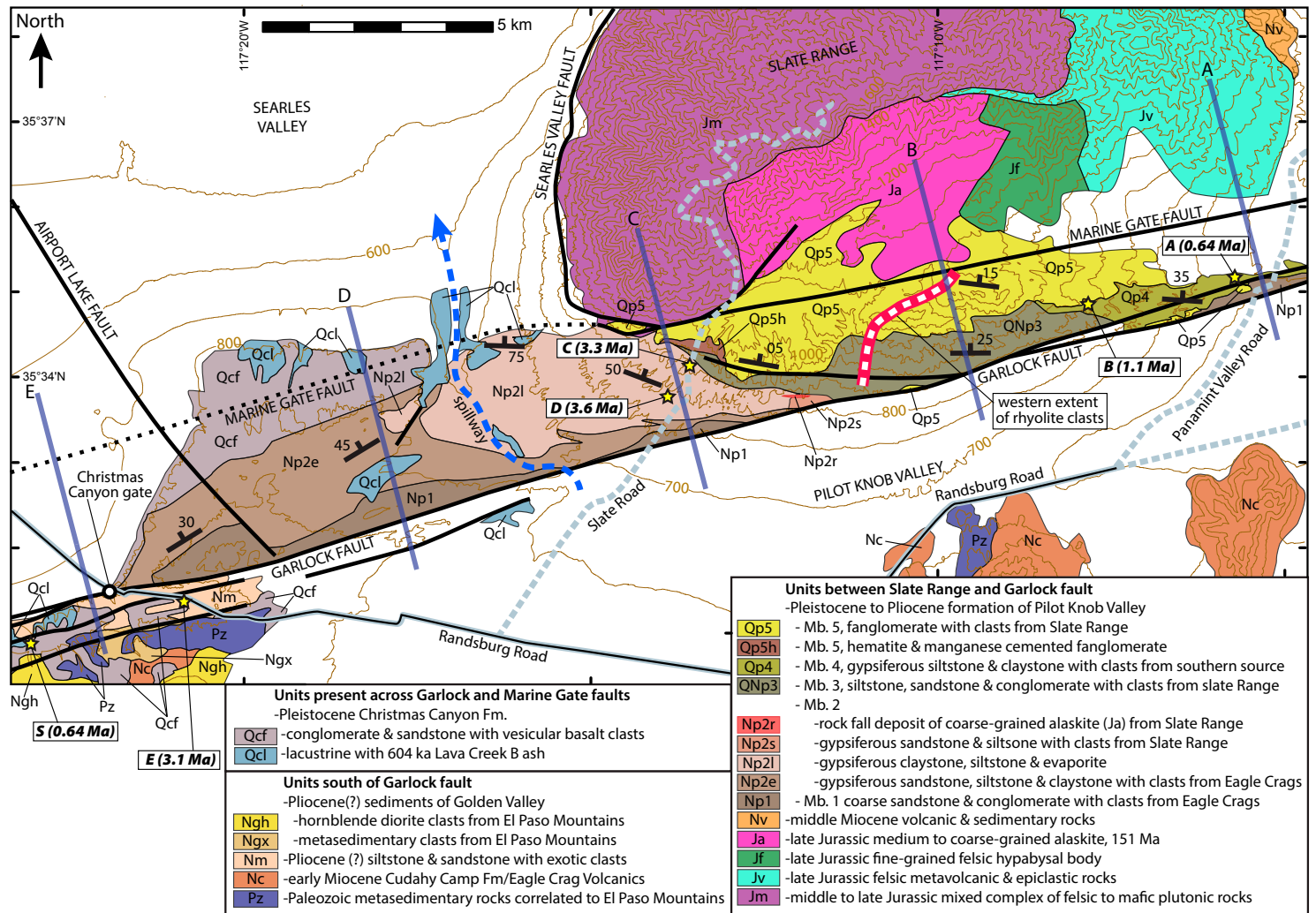
Figure 2. Simplified geologic map of the study area showing basement rocks, and the Christmas Canyon Formation and the formation of Pilot Knob Valley. Map is based on Andrew et al. (2014a, 2014b). Younger alluvial and pluvial units are white. The Airport Lake fault trace is from unpublished fieldwork by Andrew and Walker. Also shown are the locations of samples analyzed by tephrochronology. Bold dark lines running perpendicular to the outcrop trace are the locations of sections shown in Figure 7.

and fingerprint source regions for basin sediment. Identifiable clasts in the Pliocene–Pleistocene strata consist of rocks ranging from Paleozoic to Miocene in age. The recognition process requires identifying clast types, including unique textures, mineralogy, and clast assemblages. Matching clasts to sources requires understanding the lateral displacement of the sources during development and evolution of the Garlock fault system (Monastero et al., 1997; Andrew et al., 2015), similar to classic studies on the San Andreas fault of Poway clasts by Yeats et al. (1974) and Nilsen and Clarke (1975).

Eagle Crags Volcanic Field

South of Pilot Knob Valley lies the high-standing remnant of a 20.3–17.1 Ma stratovolcano-caldera complex that occupies the Eagle Crags, Pilot Knob, and Robbers Mountain areas (Sabin, 1994; Monastero et al., 1997). Sabin (1994, p. iii) mapped and identified a "series of intermediate to silicic tuffs, tabular flows, flow breccia, dikes, plugs, and hypabyssal rocks ranging from tholeiitic basalt to high-silica rhyolite" and termed this assemblage the Eagle Crags volcanic field. We particularly note the presence of locally abundant flow-banded dacite to rhyolite. Due to the distinctive character of this sequence, clast provenance provides important constraints on the cumulative displacement history of the Garlock fault (following work of Monastero et al., 1997; Frankel et al., 2008; Andrew et al., 2015). This suite intrudes and nonconformably overlies Mesozoic plutonic and Paleozoic eugeoclinal rocks that crop out in southern Pilot Knob Valley (Carr et al., 1992). These rocks contain distinctive schist and quartzite units as well as tectonized diorite. The combination of the distinctive volcanic rocks with older Mesozoic and Paleozoic rocks provides a readily identifiable and unique clast assemblage that can be tied to the Eagle Crags area.

Southern Slate Range

The north-south–oriented Slate Range bounds the north side of Pilot Knob Valley (Fig. 1). The bedrock units at the southern end of the Slate Range are: (1) a Middle Jurassic mixed plutonic suite of monzonite, hornblende diorite, leucogranite, and granodiorite; (2) a Late Jurassic alaskite; (3) a Late Jurassic biotite granite; (4) a Late Jurassic meta-andesite and volcaniclastic assemblage, which includes a distinctive felsite and/or meta-rhyolite in the southeastern Slate Range; and (5) middle Miocene volcanic and sedimentary rocks along the eastern range flank. Metavolcanic and older plutonic rocks have distinctive gneissic L-S tectonite fabrics (Dunne and Walker, 2004; Andrew et al., 2014a). These L-S tectonites, combined with the alaskite and meta-rhyolite, yield a unique clast assemblage sourced from the southern Slate Range.

FORMATION OF PILOT KNOB VALLEY

Approximately 2000 m of sedimentary rock are exposed as a NE-tilted block bound by the Garlock fault to the south and the Slate Range to the north, with exposure along the entire southern end of the Slate Range (Figs. 2 and 3). We place these sedimentary rocks into the formation of Pilot Knob Valley (PKfm, defined originally in Andrew et al., 2014a) by using regional stratigraphic correlations and new age data (this paper and in Andrew et al., 2015) along with extensive recent geologic mapping (Smith, 2009; Rittase, 2012; Andrew et al., 2014a, 2014b). Although the PKfm is locally faulted and folded, we interpret it as a single depositional package. We do not present a measured section due to internal deformation and strong lateral lithologic and facies variations. Instead, we present a vertically and laterally consistent stratigraphic framework (Fig. 4). The thickness of units can be locally measured but is mostly estimated using the dip and map thickness. We do the same in deformed units but try to take into account repetition by folding or faulting. Facing indicators are ubiquitous in all of the units. Brief descriptions of these rocks were first published in Noble (1931, p. 10–13) but without accompanying detailed mapping or described section. We divide the PKfm into five members based on provenance and lithologic

characteristics. Details of age interpretations are given in subsequent sections. Descriptions of rock types are presented below, and outcrop relations are shown in Figures 2 and 4. Summary descriptions of the units are given in Table 1.

Member 1 (Np1)

Member 1 comprises the lowest exposed rocks of the PKfm and consists of conglomerate and coarse sandstone with mixed mafic to banded felsic volcanic clasts (Figs. 5A, 5B, and 6A–6C). Member 1 forms low-relief hills that are mantled by a lag of weathered-out clasts. The surface of member 1 has a distinctive gray-blue hue indicative of the numerous dacitic lava clasts present in this unit. Fresh exposures along cut banks are more salt-and-peppered to dark-gray colored.

Bedding is typically crude east of the Randsburg Wash–Searles Valley spillway (blue dashed line in Fig. 2), where the deposit is mostly coarse sand. Bedding becomes obscured within an ~50-m-wide swath near the Garlock fault. The unit is coarser grained and better bedded between the spillway and Christmas Canyon gate. Beds are up to 30 cm thick, and the deposit is locally clast supported near Christmas Canyon gate. Clasts are up to 20 cm in diameter but commonly 2–10 cm across. Up to 5% of the clasts are gray monzonite composed of phaneritic grains of predominately feldspar but also biotite and euhedral hornblende phenocrysts up to 3 mm, possibly sourced from Robbers Mountain (Carr et al., 1992) on the north flank of Eagle Crags. The monzonite clasts lack foliation.

Member 2 (Np2)

Member 2 is generally finer grained than Member 1 and consists mostly of sandstone, siltstone, mudstone, and evaporite. It is locally primarily mudstone and evaporite, but these rocks grade laterally into coarser conglomerate and sandstone with different clast composition assemblages. Grain size and clast composition vary and allow division of Member 2 into 4 subunits.

Figure 3. Annotated field photograph showing uplifted late Cenozoic sediments in northern Pilot Knob Valley. View is looking northeast. Heavy-weight line marks the Garlock fault, and arrows indicate slip direction. Medium-weight lines separate sedimentologic and lithologic facies as labeled. Thin dashed line marks top of fanglomerate hilltop in front of Slate Range. fangl.—fanglomerate; Rx.—rocks; ss.—sandstone; seds.—sediments.

Subunit 2e—Gypsiferous Sandstone, Siltstone, and Mudstone with Eagle Crag Clast Source (Np2e)

Subunit 2e consists of gypsiferous sandstone, siltstone, and mudstone. Pebbles, typically less than 1 cm across and well rounded, occur in some sandstone beds and consist of mafic and porphyritic intermediate volcanic clasts derived from Eagle Crags (Sabin, 1994; Monastero et al., 1997). This subunit (Figs. 2 and 5C) occurs along and stratigraphically below the southern exposure of subunit 2l, a distinctively finer-grained unit (see below), but locally interfingers with it. The contact is gradational both upward in section and laterally to the west. Because of the finer-grained

nature of the deposit, subunit 2e is more easily erodible than member 1 and weathers to form slopes north of Christmas Canyon gate. Along Slate Road, subunit 2e weathers similarly to subunit 2l but appears slightly darker in color and forms less nubby outcrops.

Subunit 2l—White Siltstone, Mudstone, and Evaporite (Np2l)

Subunit 2l consists of light-colored and well-bedded gypsiferous sandstone, siltstone, and mudstone (Figs. 2, 5D, 5E, and 6D). At least ~750 m of section is exposed near Slate Road (location shown on Fig. 2). However, the true depositional

thickness of subunit 2l is difficult to measure due to abundant folding and faulting of this unit. These rocks are relatively well-indurated, but clay-rich beds are generally poorly exposed and commonly weather at the surface in a popcorn-like texture (Fig. 6D). Karstification is common at ravine bottoms due to alluvial runoff dissolving salt deposits and other soluble constituents (Fig. 5D). Sandstone beds locally contain a few pebbles less than 0.5 cm in size with a Slate Range provenance consisting of dark gray-green metasedimentary and alaskite assemblages. Numerous probable ash layers are exposed throughout the section, but many are reworked or altered to yellowish mudstone. These ash beds make excellent markers to define structural geometries and provide an opportunity to
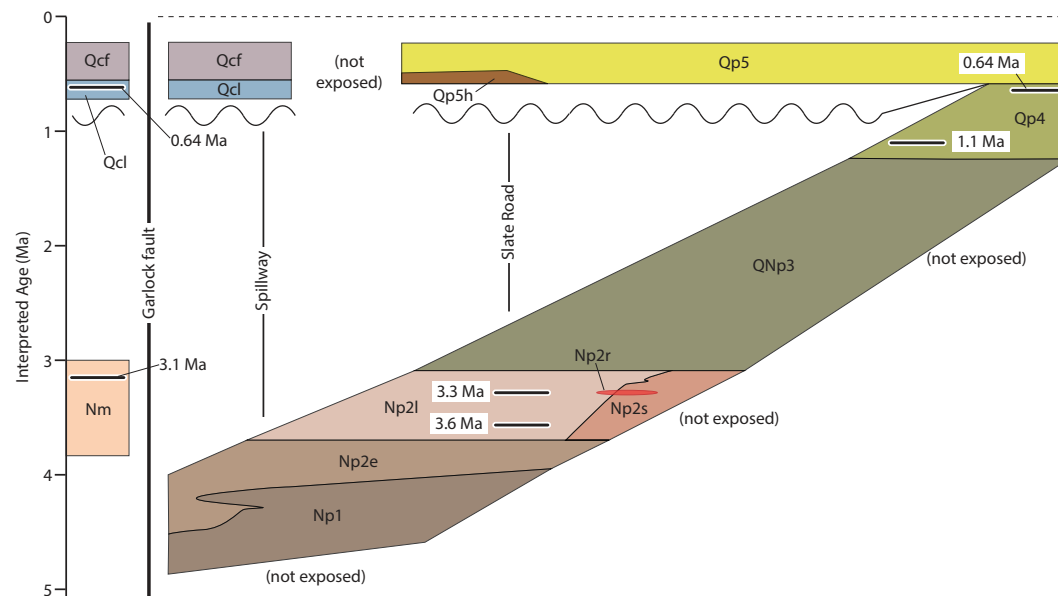
Figure 4. Generalized distribution and ages of rocks discussed in this paper and shown in Figure 2. Only late Cenozoic rocks are depicted. The diagram shows the schematic relations from west to east across the area. Ashes with interpreted ages are shown in black. Ages are rounded to the nearest 0.1 Ma. Most contacts are considered conformable except the unconformable bases of member 5 and the Christmas Canyon Formation.

TABLE 1. UNITS IN PILOT KNOB VALLEY PLIOCENE TO PLEISTOCENE SECTION

| Unit	Rock Types	Clasts and Provenance	Depositional Environment
Np1	Conglomerate and coarse sandstone	Mixed mafic to felsic volcanic rocks, rate monzonite. Eagle Crags source.	Northward prograding alluvial fans
Np2e	Gypsiferous sandstone, siltstone, and mudstone	Mafic to intermediate volcanic rocks. Eagle Crags source.	Lacustrine and marginal lacustrine
Np2l	Mudstone, siltstone, and evaporite	Local sandstone beds with metaigneous material. Slate Range source?	Lacustrine
Np2s	Sandstone to siltstone interbedded with sandstone to pebble conglomerate	Mostly meta-igneous rocks and lesser mafic to felsic volcanic rocks. Mixed Slate Range and Eagle Crags sources.	Lacustrine and marginal lacustrine
Np2r	Megabreccia	Granite and metaigneous rocks. Slate Range source.	Rock fall
Nm	Siltstone, sandstone, pebble conglomerate	Mafic to intermediate volcanic rocks, metasedimentary rocks including quartzite. Source in Eagle Crags and Robbers Mountain	Alluvial fan
QNp3	Conglomerate, sandstone, siltstone	Meta-rhyolite, L-S tectonite of metaigneous rocks, gneiss, and granite. Slate Range source.	Alluvial fan into lacustrine
Qp4	Gypsiferous siltstone and mudstone	Meta-rhyolite, granite, vesicular basalt. Mixed Slate Range source with Black Hills?	Lacustrine and marginal lacustrine
Qp5	Conglomerate	Granite, gneiss, schists, meta-rhyolite. Slate Range source.	Alluvial fan, bajada
Qp5h	Conglomerate, hematite and magnesium-oxide stained and cemented	Granite, gneiss, schists, meta-rhyolite. Slate Range source.	Alluvial fan, bajada, hydrothermal fluids
Qcl	Mudstone and siltstone	None	Lacustrine
Qcf	Conglomerate	Mixed volcanic and metaplutonic rocks, quartzite and vesicular basalt. Reworked from all underlying units.	Coluvial surface
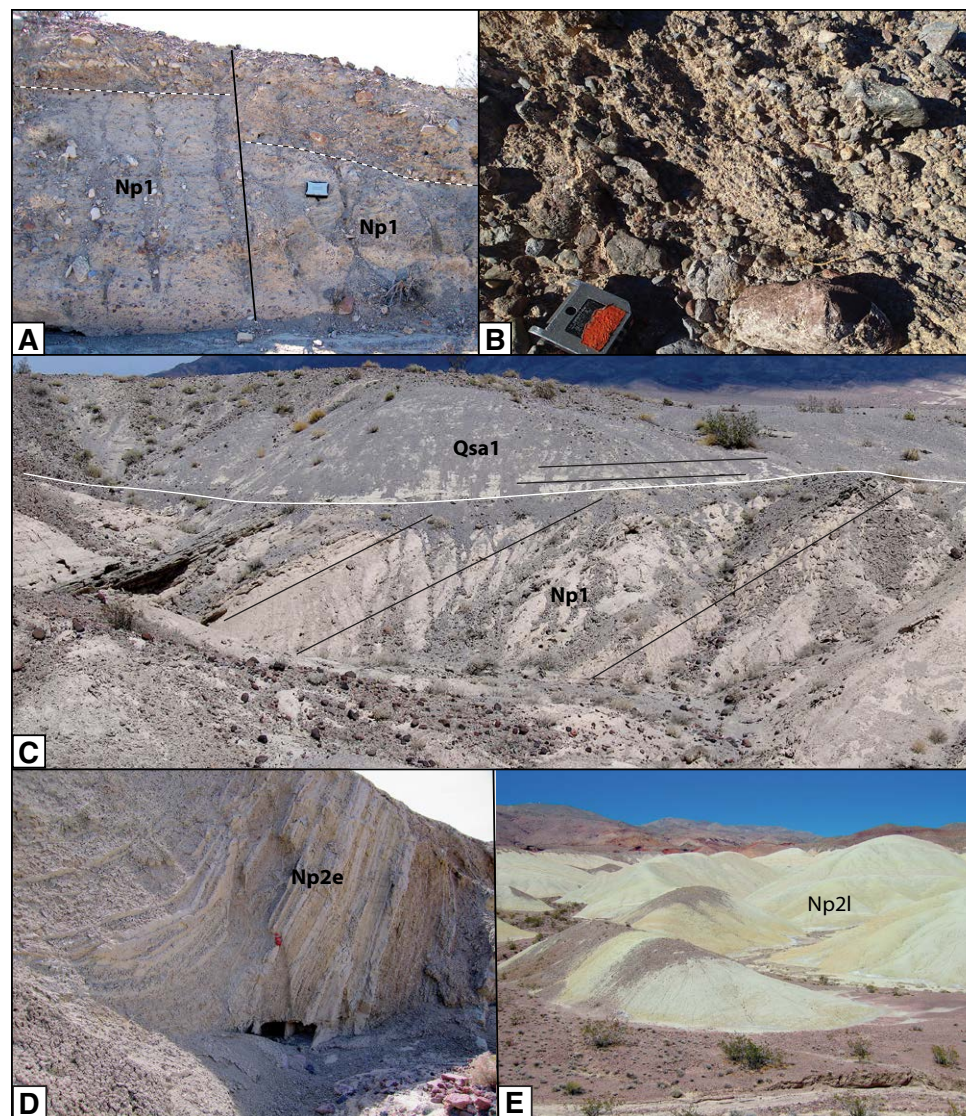
Figure 5. Annotated photographs showing key stratigraphic and weathering features of the formation of Pilot Knob Valley. (A) Lower distal conglomerate and sandstone of member 1. (B) Close-up of Member 1 showing andesitic volcanic clasts (bottom of photo and right of the compass) and generally rounded nature of the material. Note crude layering in the unit. (C) Lower member 1 dipping ~45°N, capped unconformably by subhorizontal Searles Valley Formation lacustrine sediments (Qsa1 of Smith, 2009). Photo was taken ~2 km west of Randsburg Wash–Searles Valley spillway. View is looking north. (D) Close-up of folded white siltstone and mudstone beds (member 2, subunit 2l). Rocks weather to popcorn-like surface on left. Note the fine-grained and thinly bedded nature of the unit. (E) White outcrops of member 2. Here rock is more massively layered and has low-relied outcrop. Photo taken ~1 km west of Slate Road. (*Continued on following page.*)

partially reconstruct stratigraphic sections of this strongly deformed unit.

Subunit 2s—Conglomerate to Siltstone of Mixed Eagle Crags and Slate Range Clast Sources (Np2s)

This is a poorly sorted and graded, fine-grained sandstone and siltstone unit interbedded with coarse-grained arkosic sandstone and pebble conglomerate. This unit grades laterally into submember 2l to the west. Unlike other coarse-grained units, this unit contains mafic to intermediate porphyritic extrusive rocks, gneiss, alaskite, and undifferentiated dark-colored metasedimentary clasts derived from both the Slate Range and Eagle Crags. This unit is poorly exposed adjacent to the Garlock fault, and facing indicators are obscured by deformation. We estimate this subunit to be 50–80 m thick based on outcrop extent. Relative abundances of clast types appear to be ~80% Slate Range lithologies and 20% Eagle Crags mixed volcanic rock types.

Subunit 2r—Rock Avalanche Deposit from the Slate Range (Np2r)

Megabreccia crops out locally as a 1–5-m-thick layer within the upper, interfingered portion of subunits 2l and 2s (Fig. 5F). It consists of mostly pink-weathering coarse granite and ~5% dark greenish-black metamorphic rock (Fig. 6E). The heavily fractured nature of the clasts and the presence of scaly sediments at its base suggest a rock avalanche transport mechanism. The clast types correlate with Jurassic rocks along the southern flank of the Slate Range.

Members 3, 4, and 5

These members occur east of the Randsburg Wash–Searles Valley drainage divide (Fig. 2). Members 3 and 5 are composed mostly of sandstone and conglomerate with member 4 present as
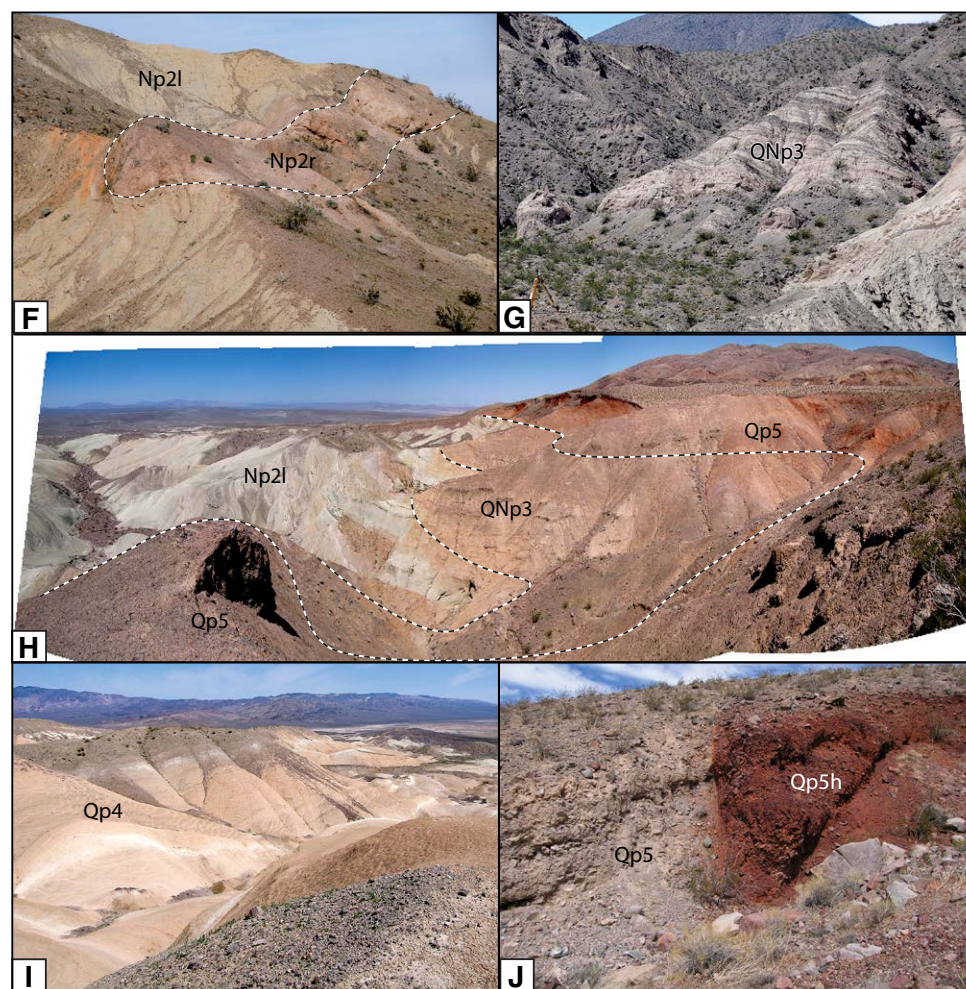
intervening and intercalated beds of mudstones to finer-grained sandstones (Fig. 4).

Member 3—Conglomerate, Sandstone, and Siltstone Unit (QNp3)

Member 3 is well-bedded siltstone, sandstone, and conglomerate unit with clasts of meta-igneous rocks sourced from the southern Slate Range (Figs. 5G and 5H). Siltstone and sandstone dominate the lower portions of this unit. The upper half of this unit includes conglomerate with clasts of meta-rhyolite, white-colored granite, light-colored gneiss or mylonite, red-colored granite, and bluish-green gneiss (Fig. 6F and 6G). Unit thicknesses vary greatly from east to west, but it is at least 200 m thick adjacent to the south-central Slate Range.

Bedding thicknesses range from 2 to 10 cm at the bottom to up to 0.5 m at the top. The bottom of member 3 sits conformably on subunit 2l, and bedding dips gradually decrease upsection. Syn-tectonic deposition and increased mechanical strength of these thick clastic sediments compared to the finer-grained unit below likely caused fanning of dips documented in this unit. Member 3 pinches out to the west where member 5 and subunit 5h sit locally unconformably on subunit 2l; member 3 thickens dramatically to the east before grading laterally into member 4 (Fig. 2). Member 3 is more resistant to erosion than underlying deposits and forms a noticeable break in slope with the finer-grained lacustrine deposits. This unit is red to orange in color.

Figure 5 (*continued*). (F) Pink granite and black metasedimentary rock avalanche deposit (member 2, subunit 2r) within member 2. See Figure 2 for the limited outcrop area of this unit (Np2r). (G) Lower conglomerate and sandstone of member 3. Photo just north of outcrops of Np2r. (H) Panoramic view looking west in the central part of the field area. White subunit 2l is overlain by red weathering conglomerate of member 3 (QNp3) and flatter lying conglomerate of member 5 (Qp5). Note the apparent fanning of dips from older to younger rocks. (I) Eastward view of younger member 4 fine-grained sedimentary (Qp4) near the eastern extent of the study area. White layers are altered ash beds. (J) Upper proximal conglomerate of member 5. Here, conglomerate of unit Qp5 is faulted against hematite- and manganese-stained conglomerate of subunit Qp5h on right.

Member 4—Brown Gypsiferous Siltstone and Mudstone Unit (Qp4)

The fourth member of the PKfm is composed of mudstone, siltstone, and sandstone grading upward into a pebble conglomerate. A distinctive brown mudstone occurs in the lower portion of this unit (Fig. 5I). The upper conglomerate is matrix-supported and contains clasts of meta-rhyolite, red granite, white-gray granite, slate, schist, and also
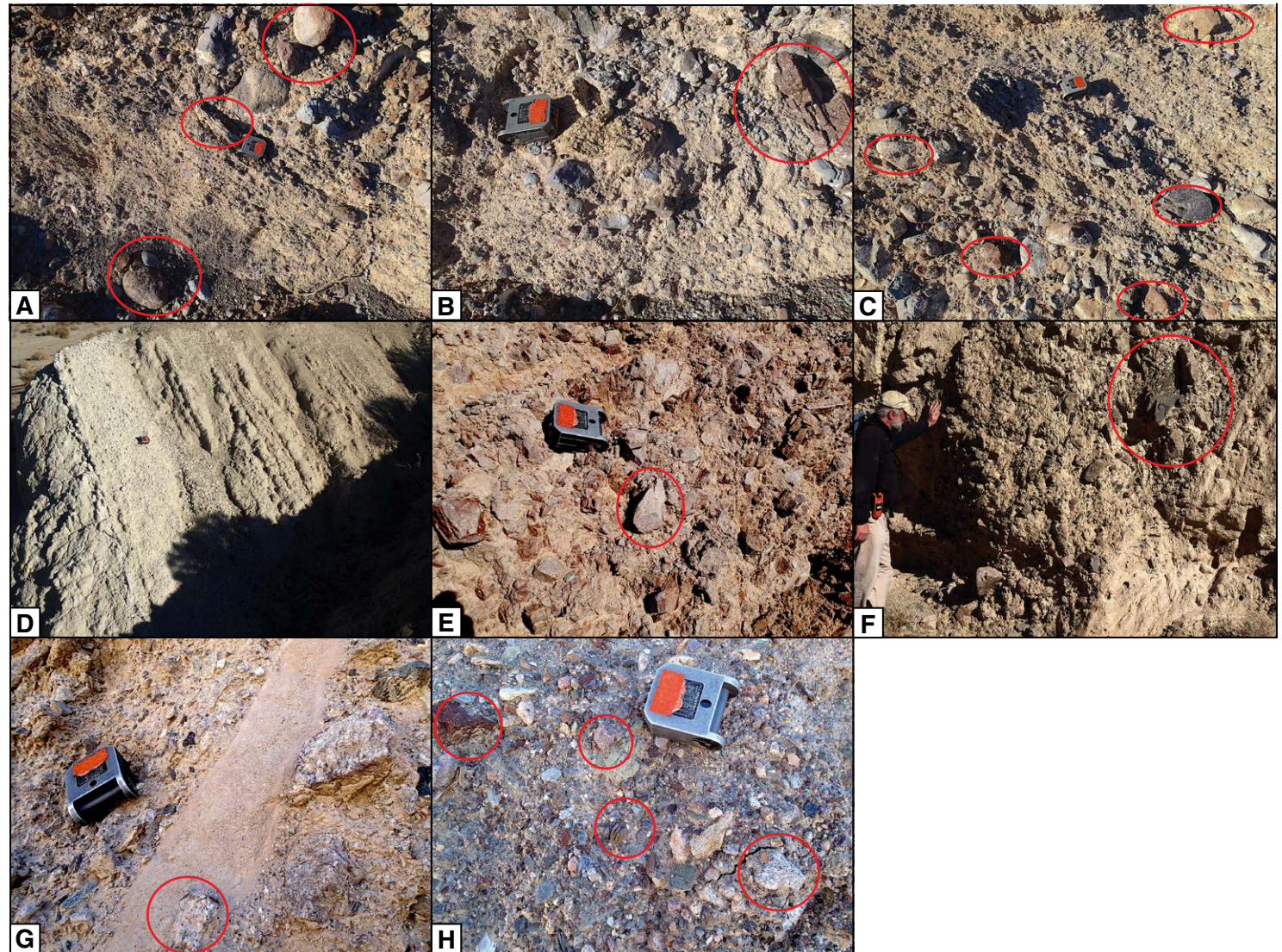
Rittase et al. | Pilot Knob Valley

Figure 6. Detailed field photographs showing clast types in the units of the formation of Pilot Knob Valley. Note: Brunton compass in photos is ~7 cm². (A) Member 1. From left to right, intermediate volcanic rock, schist, intermediate and felsic volcanic rocks. All clasts are distinctly rounded. (B) Member 1. Red weathering volcanic clast. (C) Member 1. Rounded clasts of volcanic rocks. Note glassy texture of clast in middle right. (D) Member 2, subunit 2l. Note popcorn texture weathering pattern. (E) Member 2, subunit 2r. Angular clasts in megabreccia. (F) Member 3. Coarse conglomerate of gneissic metavolcanic and plutonic rocks. Note angular clasts in upper-right circle. (G) Member 3. Granite plutonic clasts identical to rocks in the southern face of the Slate Range. (H) Member 4. From left to right, red volcanic clast, felsic volcanic rock, metasedimentary clast, and granite clast.

Rittase et al. | Pilot Knob Valley

vesicular basalt, plagioclase-rich basalt, gray dacite and/or andesite, and red plagioclase-rich basaltic-andesite (Fig. 6H). The volcanic rocks appear to be derived from the Eagle Crags to the south of Pilot Knob Valley. The fine-grained lacustrine deposits of member 4 erode easily and form large rounded mounds. White ash beds within these mounds allow a sense of bedding orientation. This unit weathers similarly to subunit 2l to the west. Furthermore, the conglomerate beds in this unit are resistant to erosion, forming steeper slopes and protective caps over underlying mudstones. Locally, the top of the unit has a slight angular unconformity with member 5. Member 4 is estimated to be ~175 m thick.

Member 5—Conglomerate Unit of Slate Range Material (Qp5)

Member 5 is a thick and aerially extensive coarse conglomerate at the top of the PKfm. The thickness of this unit varies across the study area but is probably in excess of 300 m in the central part (Fig. 2). Smith et al. (1968) mapped this member as their unit "Qg," but this paper places it within the PKfm. Smith et al. (1968) were motivated by the clear angular unconformity at the base of the unit in western sections of Member 5. Our mapping, on the other hand, traces this contact eastward into an interfingering and conformable contact. For this reason, and as explained below and shown on subsequent figures, we consider Member 5 to be part of the PKfm, but that it also records diachronous and spatially distinct deformation during deposition. We emphasize that the basin developed coeval with faulting; so it is reasonable to interpret parts of the section as conformable throughout, whereas other areas may contain distinct breaks.

Unlike older PKfm member units, member 5 deposits are less deformed and generally have low dip angles between 0° and 10°. Beds range in thickness from 10 cm to greater than 1 m (Fig. 5J). Sorting and grading of clasts are poor. This unit is mostly matrix-supported but locally clast-supported. Clast size ranges from pebbles to boulders greater than 1 m in diameter. These conglomerates contain clasts of granite, quartz monzodiorite, gneiss, schist, slate, and meta-rhyolite. The deposit has an overall gray color due to chlorite-bearing clasts derived from the Jurassic igneous and the metavolcanic rocks. The composition of these clasts resembles rocks directly to the north on the flank of the Slate Range. Paleoflow indicators also support a Slate Range source. The average dip is to the north to northeast, making this unit backtilted toward its source. Locally, this deposit shows a different clast composition than the modern washes and neighboring Slate Range bedrock. This is due to the fact that, presumably, some of the bedrock source areas presently exposed were covered during member 5 deposition or were laterally displaced by faulting. Member 5 is well indurated and forms ledges. To the west, it rests in angular contact on subunit 2l, whereas it merges laterally and interfingers eastward with member 4. This relation is discussed in detail below.

Subunit 5h—Hematite- and Manganese-Stained Conglomerate (Qp5h)

Subunit 5h is a 20–30-m-thick conglomerate unit composed of meta-igneous and granitic clasts locally preserved below member 5 (Figs. 5H and 5J). This unit is more lithified than all of the overlying conglomerates and has steeper dips. The clasts are commonly angular. This unit is very well indurated and commonly crops out as cliffs and overhangs. Conglomerate is mostly matrix-supported but clast-supported locally. The matrix is a coarse sandy arkose, and bedding is thick to massive. This unit has distinctive dark-red to purple hematite and manganese-oxide staining. In localized areas, thick concretions of hematite and manganese oxide completely encase the clasts and cement the sandy matrix. A similar red staining occurs in older Mesozoic basement rocks along the fault bounding the nearby southern Slate Range. This staining occurs across several contacts of meta-plutonic bodies, and the top of the hematite stain is roughly horizontal. Postdeposition hematite and manganese oxide staining is present. This staining occurred prior to termination of member 5 deposition as rare hematite- and manganese-stained clasts exist in member 5.

Correlative Facies South of the Garlock Fault (Nm)

A 100–300-m-thick Late Pliocene metasedimentary clast-rich deposit crops out south of the Garlock fault near the mouth of Christmas Canyon (Fig. 2). Based on clast provenance, this unit is similar to member 1 of the PKfm. These beds were previously included within the Christmas Canyon Formation by Smith (1964) and within the same formation and unit Ts (Tertiary sandstone and siltstone) by Smith (2009). Remapping in Andrew et al. (2014a) and new age constraints presented here lead us to group this unit within the PKfm. This unit is deformed a similar amount to the lower and middle parts of the PKfm, as evidenced by the generally steep NW and SE dips. It is composed of beds of siltstone and fine arkosic sandstone with lenses of pebble sandstone and pebble conglomerate. The clasts are a mix of basalt, intermediate volcanic rocks, hornblende diorite L-S tectonite, and metasedimentary rocks including quartzite. This clast assemblage matches the rocks along the south side of the Pilot Knob Valley, where a set of north-south–striking metasedimentary rocks (Carr et al., 1992) is overlain by the Eagle Crags volcanic rocks (Sabin, 1994; Monastero et al., 1997).

■ CHRISTMAS CANYON FORMATION (Qcf and Qcl)

The Christmas Canyon Formation was first described in Smith (1964) and remapped in Smith et al. (1968) and Smith (2009). In the Lava Mountains, these rocks contain the ca. 631 ka Lava Creek B ash (Matthews et al., 2015) and are thus late Pleistocene in age. Based on the current mapping of Andrew et al. (2014a, 2014b) and age data presented here, it is clear that Smith et al. (1968) and Smith (2009) used the name Christmas Canyon Formation for a mixture of different Pliocene and Pleistocene units. Hence, we have remapped

parts of these rocks in the Pilot Knob Valley area. Rocks shown in this paper and Andrew et al. (2014a, 2014b) as Christmas Canyon Formation are divided into fine-grained lacustrine and coarse-grained conglomerate units, a usage that conforms to the original description of the type location of these rocks in the eastern Lava Mountains (see Smith, 1964, p. 40–42). We describe these rocks below and emphasize that our intent is to be most consistent with the type section of Smith (1964).

The lacustrine member is a flat-lying, light-green to bluish mudstone and siltstone that crops out along the Randsburg Wash–Searles Valley spillway (blue line in Fig. 2). Unit thickness in the study area is ~10–15 m. It rests in sharp angular unconformity with underlying PKfm member 1 and subunit 2e (Fig. 4). The lacustrine member weathers easily and forms low-relief rounded hills that are commonly veneered by cobbles and boulders shed off neighboring conglomerate. Locally, the base of the lacustrine member is a 20–50-cm-thick, well-bedded and well-sorted, fine white silt deposit or reworked ash. Samples were collected, but no datable material was recovered.

The overlying member is ~30-m-thick, flat-lying, and poorly bedded conglomerate. The conglomerate consists of rounded plutonic and metamorphic rocks from the Slate Range and mixed volcanic rocks from Eagle Crags. Vesicular basalt cobbles and boulders are common, and well-rounded quartzite clasts are also found on the surface and probably represent modern reworking of clasts from the El Paso Mountains (e.g., Carter, 1994). Much of the conglomerate member appears to be a lag deposit derived from the underlying units of the formation of Pilot Knob Valley.

Tephrochronology Data and Age of PKfm

Five volcanic, distal ash-fall samples (T-PKV-WMR-A to T-PKV-WMR-E) were collected from PKV lacustrine sediments (Fig. 2) and submitted to the U.S. Geological Survey Tephrochronology Project Laboratory in Menlo Park, California, for geochemical determination of major- and minor-oxide abundances and for comparison with dated or chemostratigraphically constrained tephra deposits of western and central United States. An electron microprobe was used to determine the concentrations of nine oxides (SiO_2, Al_2O_3, FeO, MgO, MnO, CaO, TiO_2, Na_2O, and K_2O) to generate a geochemical fingerprint of the tephra. Statistical correlations were used to determine the closest match among a geochemical database of ~6600 dated volcanic ashes. In the absence of large phenocrysts suitable for conventional dating techniques, this method has proven to be quite robust (Sarna-Wojcicki, 2000). Locations and a summary of ages are given in Table 2. Mean chemical values used for comparison and correlation are shown in Table 3. We use the time scale of Walker et al. (2018) for comparison and age names.

Sample T-PKV-WMR-A was collected from near the top of lacustrine unit Qp4 of the PKfm (Fig. 2). This sample correlates well to the 0.631 Ma Lava Creek B ash from the Yellowstone National Park area in Wyoming. This sample has a 0.95 similarity coefficient (SC), both with and without alkalis, to Lava Creek B ash. A second plausible correlation is to the ca. 2.06 Ma Huckleberry Ridge ash (Lanphere et al., 2002). However, because sample T-PKV-WMR-A sits stratigraphically higher than T-PKV-WMR-B (discussed below), the Lava Creek B ash correlation is more reasonable.

Sample T-PKV-WMR-B was collected from near the middle of the exposed lacustrine unit Qp4 of the PKfm. It is most similar to the ca. 1.13–0.87 Ma upper tuffs of Glass Mountain (Sarna-Wojcicki et al., 2005) and the ca. 0.76 Ma Bishop Tuff. The eruptive source for both of these tuffs is the Long Valley Caldera to the north of the study area in Owens Valley, California. We, for discussion, assign the 1.13 Ma age for upper tuffs of Glass Mountain to this part of Qp4.

Sample T-PKV-WMR-C was collected from the top of unit Tp2l along Slate Road. It has similar geochemistry to the 3.26 Ma tuff of Mesquite Springs and the 3.35 Ma tuff of Zabriskie Wash. The tuff of Mesquite Springs has a slightly higher SC value than the tuff of Zabriskie Wash. The eruptive source for the tuff of Mesquite Springs is in northern Death Valley. This ash places this unit at ca. 3.3 Ma in age, or late Pliocene.

Sample T-PKV-WMR-D was collected from the middle of unit Tp2l. This sample correlates well to the >3.58 Ma tuff of Artists Drive of the lower Nomlaki family and the 3.27 Ma Nomlaki Tuff. Sample T-PKV-WMR-D sits stratigraphically lower in Tp2l and thus is older than T-PKV-WMR-C. Additionally, the tuff of Artists Drive has a slightly higher SC value. The eruptive sources for the tuff of Artists Drive and the Nomlaki Tuff are in the southern

TABLE 2. TEPHROCHRONOLOGY RESULTS

Sample	Location	Most similar unit	Assigned age (Ma)
T-PKV-WMR-A	−117.093°, 35.587°	Lava Creek B, Wyoming	0.631
T-PKV-WMR-B	−117.130°, 35.582°	Upper tuffs of Glass Mountain, California	1.13
T-PKV-WMR-C	−117.225°, 35.569°	Tuff of Mesquite Springs or tuff of Zabriskie Wash, California	Ca. 3.3
T-PKV-WMR-D	−117.231°, 35.563°	Tuff of Artists Drive, California	3.58
T-PKV-WMR-E	−117.346°, 35.523°	Coso Range, California	3.14

TABLE 3. CHEMICAL DATA FOR TEPHROCHRONOLOGY SAMPLES

Sample	SiO_2	Al_2O_3	Fe_2O_3	MgO	MnO	CaO	TiO_2	Na_2O	K_2O	Total
T-PKV-WMR-A	77.95	12.79	1.65	0.03	0.05	0.57	0.14	2.72	4.10	100.00
T-PKV-WMR-B	77.97	13.24	0.71	0.05	0.05	0.55	0.06	2.71	4.66	100.00
T-PKV-WMR-C	78.56	13.43	0.73	0.05	0.08	0.48	0.07	2.02	4.59	100.01
T-PKV-WMR-D	78.38	13.95	1.15	0.22	0.08	0.87	0.19	2.64	2.52	100.00
T-PKV-WMR-E	76.97	13.97	0.54	0.04	0.07	0.69	0.05	2.96	4.72	100.01

Cascades of California (Knott et al., 2008). We use the ca. 3.6 Ma date for the age of this part of unit Np2l.

Sample T-PKV-WMR-E was collected from unit Nm. It is most similar to a 3.14 Ma Coso eruptive center tephra using alkali and non-alkali oxides. A second, slightly weaker correlation using non-alkali oxides is to the 2.9 Ma Mount Jackson (Nevada) tuffs and the <2.89 to >2.58 Ma lower tuffs of the Badlands. The calcium-oxide concentrations in the Mount Jackson and Badlands samples are somewhat lower than those of T-PKV-WMR-E. Titanium oxide, in particular, is much higher in the lower

Badlands samples. Conversely, the calcium concentrations for the Coso eruptive center tephra matches are closer. This further supports the premise that the age of T-PKV-WMR-E is closer to 3.14 Ma, and that unit Nm is age equivalent to unit Np2.

■ DEPOSITION AND TECTONICS OF THE FORMATION OF PILOT KNOB VALLEY

The geology described above is shown in a fence diagram view in Figure 7. The PKfm is sandwiched presently between the Garlock and Marine

Gate faults and is being actively deformed between these structures. The basin continues westward into the subsurface, and strata are well imaged in seismic profile (Monastero et al., 2002). Monastero et al. (2002) interpreted a major reverse fault in this area, the Spangler Hills thrust, but it is clear from new mapping that their Spangler Hills thrust is the westward projection of the Marine Gate fault because the two faults are along strike from each other and exhibit very similar vertical separation. Thus, the two faults are now recognized as part of the regionally extensive Marine Gate fault (Andrew et al., 2014a). The basement beneath the PKfm is
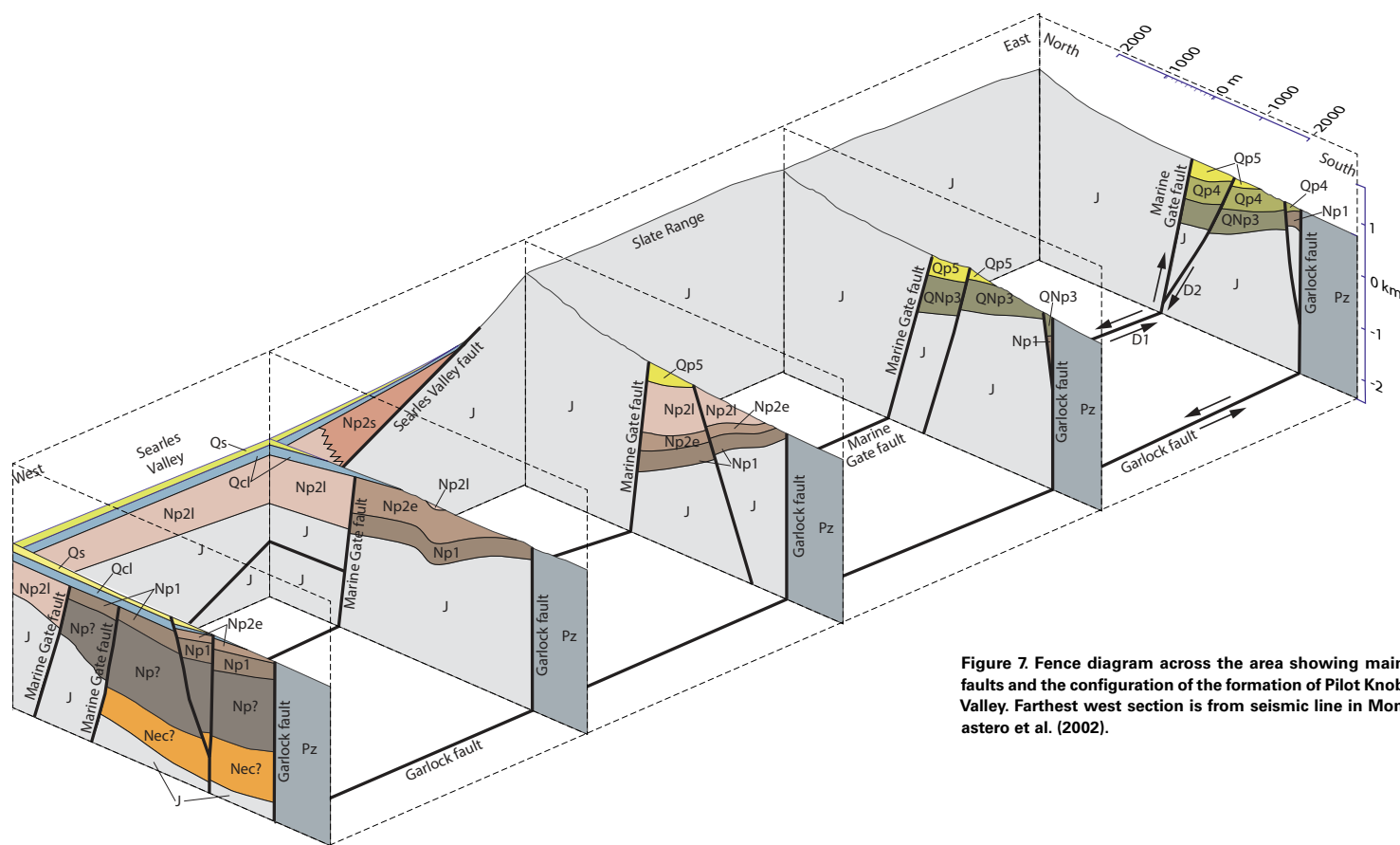

Figure 7. Fence diagram across the area showing main faults and the configuration of the formation of Pilot Knob Valley. Farthest west section is from seismic line in Monastero et al. (2002).

uncertain, but it is most reasonably interpreted as Jurassic plutonic rocks that form most of the adjacent ranges (Walker et al., 2002).

Development of the PKfm basin records the interaction between sedimentation and faulting on the Garlock, Marine Gate, and Searles Valley fault systems, and sediment sources reflect topographic changes as well as lateral motions caused by these faults. Our interpretation of the generalized geologic and paleogeographic development of the basin and sources is shown in Figure 8 for the current configuration back to 4 Ma (Figs. 8A–8C). In the Slate Range, Argus Range, Lava Mountains, and Eagle Crags, the top of the Cenozoic section consists of Miocene to Pliocene volcanic rocks almost all exclusively older than the PKfm (Monastero et al., 1997; Andrew and Walker, 2009; Andrew et al., 2015). Hence, the PKfm is deposited in a localized basin different from the extent of older deposits.
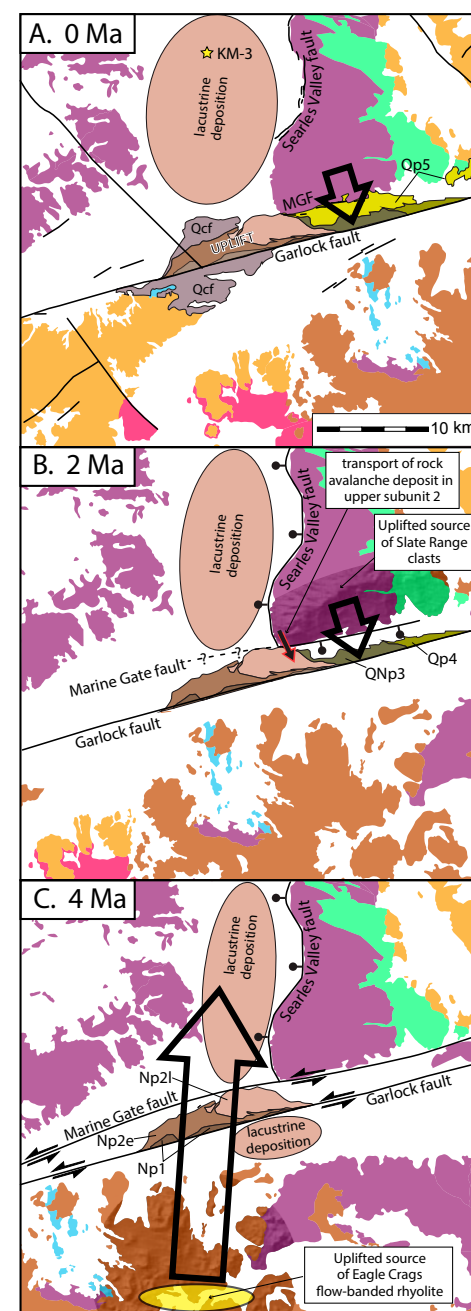
The oldest exposed rocks in the PKfm are conglomerates of Tp1. These are sourced from the Eagle Crags volcanic field and are older than the 3.6 Ma age of the overlying unit (Fig. 8C). At this time, deposition was dominated by northward-prograding alluvial fans. These rocks are not directly dated, but because they grade upward into Tp2 units, we infer that it is probably no older than ca. 5 Ma or earliest Pliocene. Taking rates of Garlock fault motion from Andrew et al. (2015) these rocks north of the Garlock fault were ~25 km farther east and much nearer to the Eagle Crags area during deposition (Fig. 8C).

The PKfm fines upward into subunits 2e, 2s, and especially 2l. These fine-grained rocks are lacustrine-facies rocks consisting of mudstone, siltstone, and evaporite. Pebble compositions show that the Eagle Crags area remains a sediment source, but the clasts from the Slate Range become a contributor in eastern parts of the section (Fig. 8B). The rock avalanche deposit in the eastern exposed section can be matched to a distinctive Jurassic intrusive rock that crops out only on the southern face of the Slate Range. The exposure is limited laterally east-west by intrusive contacts and is structurally overlain by the Layton Well thrust (Dunne and Walker, 2004; Andrew et al., 2014a). Therefore, the source for the rock avalanche deposit is unique, and

it implies newly created topographic relief on the Slate Range in the Pliocene at 3.3–3.6 Ma (ages of Np2l). Hence, the PKfm basin deepened and started seeing deposition from rocks sourced to its north, not just from Eagle Crags to the south during this time. Topographic relief was sufficient at the southern boundary of the Slate Range to mobilize rock avalanche deposits.

The overlying units represent two coarsening-upward packages. Member 3 is interpreted to be Slate Range alluvial deposits that overlap a lacustrine basin at its base. Our interpretation for this unit is that it was deposited in a similar setting to the modern range physiography, a bajada shed from steep outcrops on the southern Slate Range intersecting a basin (Fig. 8B). Members 4 and 5 interfinger and represent contributions from both southern and northern sources, respectively. Member 5 is also interpreted to represent a southward-shed bajada from the Slate Range and is identical in texture and composition at its top to the Holocene (modern) alluvium (Fig. 8A). The age of member 3 is uncertain but must lie between 3.3 and 1.1 Ma. Members 4 and 5 are ca. 1.1 Ma and younger and are thus Pleistocene in age.

Figure 8. Paleogeographic and paleogeologic map of basin development in the Pilot Knob Valley area. Fault restorations follow those in Andrew and Walker (2009) and Andrew et al. (2015). (A) The current setting with the basin uplifted and receiving sediment input from the Slate Range to the north (large open arrow shows primary sediment sources). The rock units are modified from Walker et al. (2002). Dark lines are fault scarps modified from U.S. Geological Survey fault activity map. (B) Restoration of left-lateral motion along the Garlock fault and normal slip on the Marine Gate and Searles Valley faults back to 2 Ma. The significant sediment source of the southern Slate Range is noted by the shaded relief background. Note the source and transport path for the rock avalanche deposit in the upper portion of the lacustrine subunit 2 off of the southwestern Slate Range, shown in red and black arrow. (C) Restoration of left-lateral fault motions on the Garlock and Marine Gate faults and normal motion on the Searles Valley fault to 4 Ma. There is communication between the Eagle Crags source (with shaded relief background) and clast deposition in Searles Valley (as seen in drill core KM-3) at this time indicated by the large open arrow. Note significant restored motion on the Garlock fault. MGF—Marine Gate fault.

The base of member 5 is confusing in that it is mapped as rocks of low dip resting on deformed Pliocene strata of subunit 2l to the west and interfingers with member 4 to the east. We interpret this to represent deformation of the older Pleistocene to Pliocene rocks of Np1 and Np2 in the western part of the area coeval with deposition of younger units in the eastern part. In other words, the unconformity at Slate Road becomes a correlative conformity in the eastern part of the exposure. This fits well with the observed dips and deformation of the unit. At Slate Road, there is a clear angular unconformity of the modestly tilted member 5 on subunit 2l. This contact is ~2 km north of the Garlock fault. In the eastern part, the exposures merge into the Garlock fault, and all units have similar moderate to steep dips. Therefore, our interpretation is that the western portion of the basin was deformed and eroded at the same time it was seeing continuous deposition or at least no deformation to the east (Fig. 8A). Whether members 3 and 4 were deposited to the west and eroded or not present at all because of deformation and uplift of older units is uncertain.

Relation to Fault Motions

The PKfm basin development is controlled by the Garlock, Marine Gate, and Searles Valley faults. Depositional patterns and ages reveal each structure's role and fit well with our regional understanding of the timing of fault motion and initiation. The oldest rocks exposed are in unit Np1 and were sourced from the Eagle Crags area. Because these rocks must be older than 3.6 Ma, we restore between 20 and 30 km of slip on the Garlock fault, placing the PKfm basin adjacent to a local source in the Eagle Crags (Fig. 8). At this time, there is no deep basin associated with the Garlock fault, no sediment source in what is now the Slate Range, and there are no barriers to northward transport of sediment.

The deposition of member 2 shows a change in the depositional pattern. Subunit 2e still has a source to the south but shows evidence of deepening and possibly creation of a localized to regional lacustrine basin. This is further demonstrated by the deposition of subunit 2l between at least 3.3 and 3.6 Ma. We interpret apparent basin subsidence as driven by extensional slip along the Searles Valley fault, a low-angle normal fault that dips westward from the Slate Range beneath Searles Valley (Walker et al., 2005; Numelin et al., 2007). Thermochronology from the exposed footwall beneath the detachment suggests this structure likely initiated at ca. 4 Ma (Walker et al., 2014).

The 4 Ma timing of initiation fits the geochronology from the PKfm and subsurface data from Searles Lake in the Smith et al. (1983) report on the KM-3 drill core taken from Searles Valley (location of core shown in Fig. 8A). There, the basal strata are older than ca. 3.3 Ma (Smith et al., 1983; Knott et al., 2018) and contain conglomerates with dacite clasts unlike those exposed in surrounding ranges. Clast descriptions are similar to the Eagle Crags rocks and rocks in member 1 and subunit 2e. We suggest that the KM-3 rocks and deposition in Searles Valley began with motion on the Searles Valley fault or possibly slightly predated it. Like member 1, the basal KM-3 rocks lack material from the metamorphic and plutonic rocks of the Slate Range and plutonic complex of the Argus Range. We take this to mean that deposition started at or before 4 Ma, with little relief or exposure of the Slate Range, but an axial drainage to the basin extending from the PKfm exposures into Searles Valley possibly to the source region in the present-day Eagle Crags. The Eagle Crags area currently drains northward unimpeded to the Garlock fault, and there is no evidence of significant faults or changes in its paleogeography since the Pliocene. In addition, it is likely that the Slate Range was displaced sinistrally to block this drainage path after deposition of the lower part of the PKfm.

Slate Range clast sources become dominant with the deposition on the upper parts of unit members 2 and 3 starting after 3.3 Ma (Fig. 8B). We suggest this signals the start or renewal of motion on the Marine Gate fault, and that this structure was a transfer fault related to the intersection of the Searles Valley normal fault and the Garlock fault (Rittase, 2012). Besides exposing the Slate Range as a source, the Marine Gate and Searles Valley faults created the required topography to mobilize the rock avalanche in subunit 2r. Current motion on the Marine Gate fault is essentially dip-slip and up on the north, as documented in the offset of Pleistocene channels and surfaces. In the past, the structure must have a component sinistral motion because lacustrine rocks of member 2 are juxtaposed with basement of the Slate Range. Estimates from exposures of the fault to the east may indicate up to 20 km of net sinistral slip (Andrew, 2002). Timing of lateral motion of the fault is constrained by a multi-colored, meta-rhyolite unit in the southeastern Slate Range, which is a unique provenance match for clasts in members 3 and 5. In Figure 2, a line marks the westward extent of this clast type present in the Slate Range fanglomerate units. As the fans decrease in age upsection, the westward extent of the meta-rhyolite clasts decreases until it aligns closely with its bedrock contact. This relation implies that sinistral slip along the Marine Gate fault ceased by 1.1 Ma and perhaps had ceased after 3.3 Ma.

Sedimentation Patterns through Time

The PKfm basin developed within a regional-scale setting of faulting and sedimentation interacting with the Garlock fault zone. We show in Figure 9 the patterns of deposition coincident with initiation and continued motion on the Garlock fault. At the older times, ca. 11 Ma (Fig. 9A), the Garlock fault was not a barrier to deposition, and depositional systems crossed the zone of the future structure unimpeded. This is well shown in Monastero et al. (1997), who interpreted rocks in the Dove Spring Formation and underlying Cudahy Camp Formation to have been derived from the Eagle Crags area in middle to late Miocene time.

At ca. 7 Ma, the Dove Spring basin becomes isolated to the north of the Garlock fault and has a shift in source to a newly active normal fault along its northwestern margin (Fig. 9B). Coeval with this change is the deposition of the Bedrock Spring Formation in the Lava Mountains (Smith, 1964; Andrew et al., 2015). Also, at this time, isolated basins appear along the eastern Garlock fault.
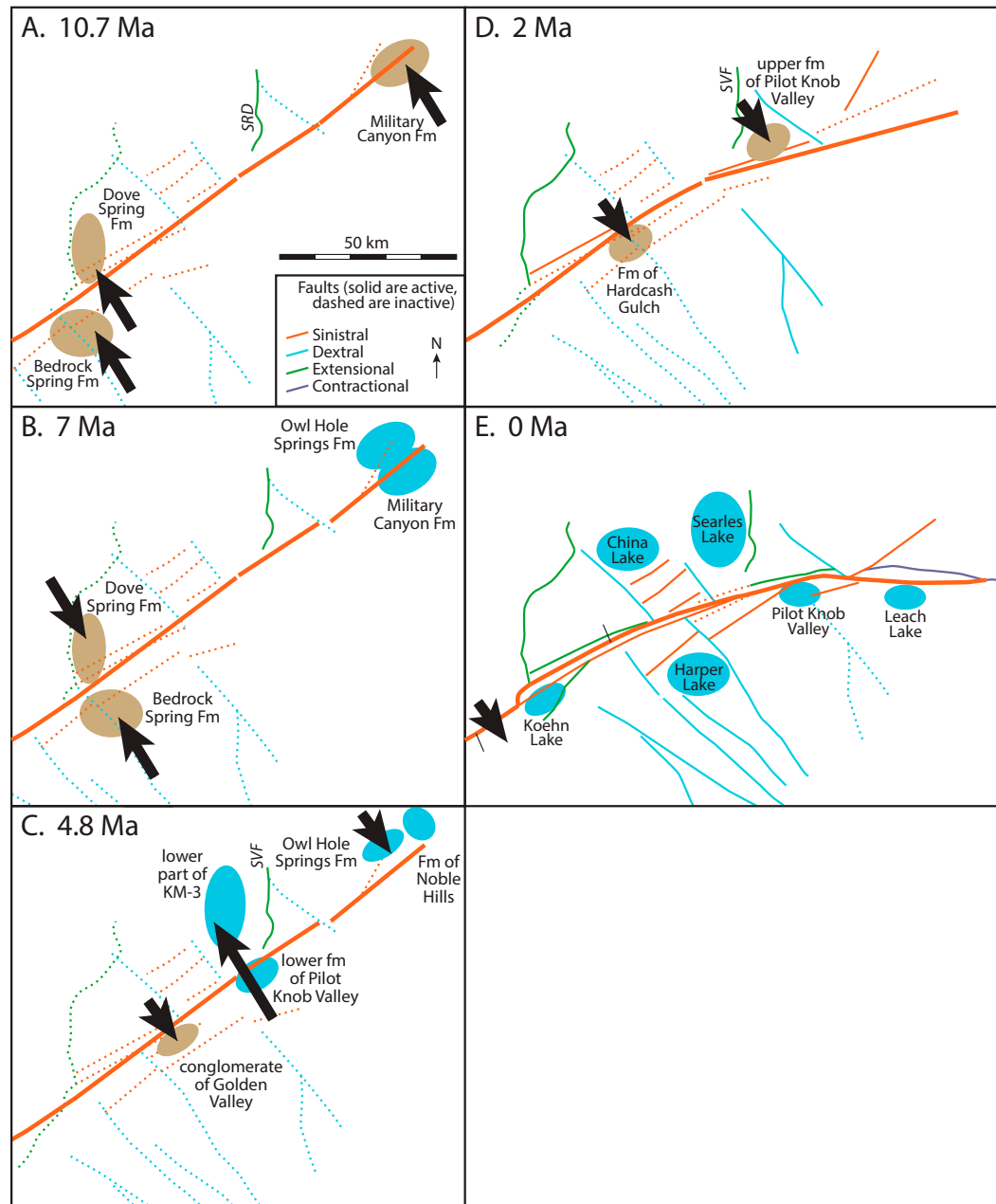
Figure 9. Time slices of the evolution of the Garlock fault zone showing sedimentation patterns, using interpreted Garlock fault zone slip history of Andrew et al. (2015) combined with new data of this paper. (A) 10.7 Ma: initiation of the Garlock fault with cross-Garlock sediment transport (black arrows). The Slate Range detachment fault initiates at this time on the north side of the Garlock fault (SRD; Walker et al., 2014). Sediment is dominated by arkosic material derived from the Mojave Desert (Brady, 1984; Loomis and Burbank, 1988; Monastero et al., 1997; Brady and Troxel, 1999; Andrew et al., 2015). (B) 7 Ma: after 10.5 km of left-lateral slip. Continued sedimentation of the Dove Spring and Bedrock Spring formations. Lacustrine basins occur at the eastern end of the Garlock, indicating a significant local disruption of the regional sedimentation pattern (Brady and Troxel, 1999). (C) 4.8 Ma: after another 19.5 km of left-lateral slip of the Garlock fault. South-derived coarse sediment transported to the lower portion of the formation of Pilot Knob Valley and found in the lower section of the Searles Lake KM-3 drill hole (Smith et al., 1983). These coarse clastic rocks are then overlain by lacustrine sedimentation from 3.6 to 3 Ma. The basin for this sedimentation is partially controlled by initiation and extension on the Searles Valley fault (SVF) at this time (Walker et al., 2005, 2014). Locally sourced clastic and lacustrine sedimentation occurs at the eastern end of the Garlock fault (Brady, 1993; Knott et al., 2005; Niles, 2016). Uplift of the El Paso Mountains dumps coarse sediment southward across the Garlock fault (Andrew et al., 2015). (D) 2 Ma: after another 9.1 km of left-lateral slip on the Garlock fault and the dextral faults of the Walker Lane belt-eastern California shear zone. Coarse clastic rocks continue to be deposited southward across the Garlock fault from the El Paso Mountains (Andrew et al., 2015). The Slate Range is uplifted and sheds sediment over the formation of Pilot Knob Valley. (E) Present day: after another 15.5 km of left-lateral slip on the Garlock fault zone and continued through-going regional dextral shear. South-directed transport occurs only on the western segment of the Garlock fault, whereas the rest of the Garlock fault zone is dominated by internal drainage with uplifted topographic shoulders and large lakes created by disruption of the regional sediment transport system.

Deposition of the PKfm began at ca. 5 Ma and is accompanied by changes in the Garlock fault (Fig. 9C). Deposition was sourced to the south, and sediment moved across the Garlock fault into the Searles Valley area. This is also about the time of initiation of uplift of the Slate Range and development of the Searles Valley fault zone (Walker et al., 2014). Although coarse clastic rocks are common, a significant change in sedimentation patterns accompanied faulting, as shown by the distribution of lacustrine rocks in the region. Another change at this time was the El Paso Mountains becoming a source with sedimentation southward across the Garlock fault (Andrew et al., 2015). Continued deposition in isolated basins continued along the eastern Garlock fault.

At 2 Ma, the Slate Range was a source into the PKfm basin, and sediment continued to be shed southward from the El Paso Mountains (Fig. 9D). The picture today is somewhat different, in that it shows mostly isolated lacustrine basins with fringing ranges shedding alluvial fans (Fig. 9E). No major transport of alluvial material occurs across the Garlock fault except in the western extent at Red Rock Canyon, western El Paso Mountains. Lake systems are interconnected with water flowing from the Owens Valley area, ultimately into the Panamint Valley and Death Valley basins.

The sedimentation patterns regionally show some variation with time. At older times before the initiation of the Garlock fault, alluvial systems freely crossed the Garlock fault. At the end of the Miocene, this pattern is disrupted, and more isolated basins are present, and the fault must present some barriers to transport. Finally, the past 5 m.y. have seen much more complicated patterns of basin development and source evolution. This complexity is formed by the simultaneous motions of the Garlock fault and eastern California shear zone.

■ CONCLUSIONS

Three general divisions can be made within the PKfm: a basal part of conglomerate containing Eagle Crags–derived volcanic clasts, a middle part that is lacustrine facies with evaporites and mudstones that grade laterally to the east to sandstone and conglomerate, and an upper sandstone and conglomerate facies with an interbedded lacustrine deposit. The presence of Eagle Crags clasts in the northern and western portions of the formation of Pilot Knob Valley indicates a continuous paleo-low north of the present Garlock fault through ca. 3.6 Ma. An overlapping and interfingering of detrital sources in the 3.6–3.3 Ma lacustrine section indicates a decrease in slope and slight southward shift in the valley's low point and/or a downstream blockage in drainage, resulting in a pluvial setting. Finally, southward progradation of coarse Slate Range fanglomerates signals a southward shift in the deepest part of Pilot Knob Valley. The upper part of the section was deposited in the past 1.1 m.y.

Deposition and deformation in the area are controlled by a complex interaction of the Garlock, Marine Gate, and the Searles Valley faults, with a possible contribution from the Airport Lake fault. Basin development reflects motion on the Searles Valley fault by widespread lacustrine deposition that probably continued northward through Searles Valley from the Pilot Knob study area. Sinistral offset on the Marine Gate fault is certainly less than 1 km in the past 1.1 m.y.

REFERENCES CITED

Andrew, J.E., and Walker, J.D., 2009, Reconstructing late Cenozoic deformation in central Panamint Valley, California: Evolution of slip partitioning in the Walker Lane: Geosphere, v. 5, p. 172–198, https://doi.org/10.1130/GES00178.1.

Andrew, J.E., and Walker, J.D., 2017, Path of dextral fault slip in the Eastern California shear zone across the central Mojave Desert: Geological Society of America Bulletin, v. 129, p. 855–868, https://doi.org/10.1130/B31527.1.

Andrew, J.E., 2002, The Mesozoic and Tertiary Tectonic History of the Panamint Range and Quail Mountains, California [Ph.D. dissertation]: University of Kansas, 154 p.

Andrew, J.E., Rittase, W.M., and Walker, J.D., 2014a, Geologic Map of the Southern Slate Range and a Portion of the Central Garlock Fault, China Lake Naval Weapons Station, San Bernardino County, California: Geological Society of America Digital Map and Chart 20, https://doi.org/10.1130/2014.DMCH020.

Andrew, J.E., Rittase, W.M., Monastero, F.M., Bidgoli, T.S., and Walker, J.D., 2014b, Geologic Map of the Northern Lava Mountains and Summit Range, San Bernardino County, California: Geological Society of America Digital Map and Chart Series, v. 19, https://doi.org/10.1130/2014.DMCH019.

Andrew, J.E., Walker, J.D., and Monastero, F.C., 2015, Evolution of the central Garlock fault zone, California: A major sinistral fault embedded in a dextral plate margin: Geological Society of America Bulletin, v. 127, p. 227–249, https://doi.org/10.1130/B31027.1.

Brady, R.H., 1984, Neogene stratigraphy of the Avawatz Mountains between the Garlock and Death Valley fault zones, southern Death Valley, California: Implications as to Late Cenozoic tectonism: Sedimentary Geology, v. 38, p. 127–157, https://doi.org/10.1016/0037-0738(84)90077-0.

Brady, R.H., III, 1993, Neogene sedimentary rocks in the southern Owlshead Mountains: Constraint on displacement of the eastern Garlock fault zone, in Sherrod, D., and Nielson, J., eds., Tertiary Stratigraphy of Highly Extended Terranes: U.S. Geological Survey Bulletin 2053, p. 25–29.

Brady, R.H., III, and Troxel, B.W., 1999, The Miocene Military Canyon Formation: Depocenter evolution and constraints on lateral faulting, southern Death Valley, California, in Wright, L.A., and Troxel, B.W., eds., Cenozoic Basins of the Death Valley Region: Geological Society of America Special Paper 333, p. 277–288, https://doi.org/10.1130/0-8137-2333-7.277.

Carr, M.D., Harris, A.G., Poole, F.G., and Fleck, R.J., 1992, Stratigraphy and structure of Paleozoic outer continental-margin rocks in Pilot Knob Valley, north-central Mojave Desert, California: U.S. Geological Survey Bulletin 2015, 33 p.

Carter, B., 1994, Neogene offsets and displacement rates, central Garlock fault, California, in McGill, S.F., and Ross, T.M., eds., Geological Investigations of an Active Margin: Redlands, California, San Bernardino County Museum Association, p. 348–356.

Dunne, G.C., and Walker, J.D., 2004, Structure and evolution of the East Sierran thrust system, east central California: Tectonics, v. 23, TC 4012, 23 p., https://doi.org/doi:10.1029/2002TC001478.

Frankel, K.L., Glazner, A.F., Kirby, E., Monastero, F.C., Strane, M.D., Oskin, M.E., Unruh, J.R., Walker, J.D., Anandakrishnan, S., Bartley, J.M., Coleman, D.S., Dolan, J.F., Finkel, R.C., Greene, D., Kylander-Clark, A., Morrero, S., Owen, L.A., and Phillips, F., 2008, Active tectonics of the eastern California shear zone, in Duebendorfer, E.M., and Smith, E.I., eds., Geological Society of America Field Guide 11, p. 43–81, https://doi.org/10.1130/2008.fld011(03).

Knott, J.R., Sarna-Wojcicki, A., Machette, M.N., and Klinger, R.E., 2005, Upper Neogene stratigraphy and tectonics of Death Valley—A review: Earth-Science Reviews, v. 73, p. 245–270, https://doi.org/10.1016/j.earscirev.2005.07.004.

Knott, J.R., Machette, M.N., Klinger, R.E., Sarna-Wojcicki, A.M., Liddicoat, J.C., Tinsley, J.C., III, David, B.T., and Ebbs, V.M., 2008, in Reheis, M.C., Hershler, R., and Miller, D.M., eds., Late Cenozoic Drainage History of the Southwestern

Great Basin and Lower Colorado River Region: Geologic and Biotic Perspectives: Geological Society of America Special Paper 439, p. 1–26, https://doi.org/10.1130/2008.2439(01).

Knott, J.R., Machette, M.N., Wan, E., Klinger, R.E., Liddicoat, J.C., Sarna-Wojcicki, A.M., Fleck, R.J., Deino, A.L., Geissman, J.W., Slate, J.L., Wahl, D.B., Wernicke, B.P., Wells, S.G., Tinsley, J.C., III, Hathaway, J.C., and Weamer, V.M., 2018, Late Neogene–Quaternary tephrochronology, stratigraphy, and paleoclimate of Death Valley, California, USA: Geological Society of America Bulletin, v. 130, no. 7/8, p. 1231–1255, https://doi.org/10.1130/B31690.1.

Lanphere, M.A., Champion, D.E., Christiansen, R.L., Izett, G.A., and Obradovich, J.D., 2002, Revised ages for tuffs of the Yellowstone Plateau volcanic field: Assignment of the Huckleberry Ridge Tuff to a new geomagnetic polarity event: Geological Society of America Bulletin, v. 114, p. 559–568, https://doi.org/10.1130/0016-7606(2002)114<0559:RAFTOT>2.0.CO;2.

Loomis, D.P. and Burbank, D.W., 1988, The stratigraphic evolution of the El Paso Basin, southern California: Implications for Miocene development of the Garlock fault and uplift of the Sierra Nevada: Geological Society of America Bulletin, v. 100, p. 12–28.

Matthews, N.E., Vazquez, J.A., and Calvert, A.T., 2015, Age of the Lava Creek supereruption and magma chamber assembly at Yellowstone based on ^{40}Ar/^{39}Ar and U-Pb dating of sanidine and zircon crystals: Geochemistry, Geophysics, Geosystems, v. 16, p. 2508–2528, https://doi.org/10.1002/2015GC005881.

Miller, M.M., Johnson, D.J., Dixon, T.H., and Dokka, R.K., 2001, Refined kinematics of the Eastern California shear zone from GPS observations, 1993–1998: Journal of Geophysical Research, v. 106, p. 2245–2263.

Monastero, F.C., Sabin, A.E., and Walker, J.D., 1997, Evidence for post–early Miocene initiation of movement on the Garlock fault from offset of the Cudahy Camp Formation, east-central California: Geology, v. 25, p. 247–250, https://doi.org/10.1130/0091-7613(1997)025<0247:EFPEMI>2.3.CO;2.

Monastero, F.C., Walker, J.D., Katzenstein, A.M., and Sabin, A.E., 2002, Neogene evolution of the Indian Wells Valley, east-central California, in Glazner, A.F., Walker, J.D., and Bartley, J.M., eds., Geologic Evolution of the Mojave Desert and Southwestern Basin and Range: Geological Society of America Memoir 195, p. 199–228, https://doi.org/10.1130/0-8137-1195-9.199.

Niles, J.H., 2016, Post-middle Pliocene tectonic development of the Noble Hills southern Death Valley, California [M.S. thesis]: San Francisco State University, 91 p.

Nilsen, T.H., and Clarke, S.H., Jr., 1975, Sedimentation and tectonics in the early Tertiary continental borderland of central California: U.S. Geological Survey Professional Paper 925, 64 p., https://doi.org/10.3133/pp925.

Noble, L.F., 1931, Nitrate deposits in southeastern California, with notes on deposits in southeastern Arizona and southwestern New Mexico: U.S. Geological Survey Bulletin 820, 108 p.

Numelin, T., Kirby, E., Walker, J.D., and Didericksen, B., 2007, Late Pleistocene slip on a low-angle normal fault, Searles Valley, California: Geosphere, v. 3, p. 163–176, https://doi.org/10.1130/GES00052.1.

Rittase, W.M., 2012, Neogene to Quaternary tectonics of the Garlock Fault and the Eastern California shear zone in the northern Mojave Desert, California [Ph.D. thesis]: Lawrence, University of Kansas, 224 p.

Sabin, A.E., 1994, Geology of the Eagle Crags volcanic field, northern Mojave desert, China Lake Naval Air Weapons Station, California [Ph.D. thesis]: Golden, Colorado School of Mines, 209 p.

Sarna-Wojcicki, A., 2000, Tephrochronology, in Noller, J.S., Sowers, J.M., and Lettis, W.R., eds., Quaternary Geochronology Methods and Applications: Volume 4: Washington, D.C., American Geophysical Union, https://doi.org/10.1029/RF004p0357.

Sarna-Wojcicki, A.M., Reheis, M.C., Pringle, M.S., Fleck, R.J., Burbank, D., Meyer, C.E., Slate, J.L., Wan, E., Budahn, J.R., Troxel, B., and Walker, J.P., 2005, Tephra Layers of Blind Spring Valley and Related Upper Pliocene and Pleistocene Tephra Layers, California, Nevada, and Utah: Isotopic Ages, Correlation, and Magnetostratigraphy: U.S. Geological Survey Professional Paper 1701, 63 p.

Smith, G.I., 1964, Geology and volcanic petrology of the Lava Mountains, San Bernardino County, California: U.S. Geologic Survey Professional Paper 457, 97 p.

Smith, G.I., 2009, Late Cenozoic geology and lacustrine history of Searles Valley, Inyo and San Bernardino counties, California: U.S. Geological Survey Professional Paper 1727, 115 p, https://doi.org/10.3133/pp1727.

Smith, G.I., Troxel, B.W., Gray, C.H., Jr., and Von, H.R., 1968, Geologic reconnaissance of the Slate Range, San Bernardino and Inyo counties, California: Special Report, California Division of Mines and Geology, v. 96, p. 1–33.

Smith, G.I., Barczak, V.J., Moulton, G.F., and Liddicoat, J.C., 1983, Core KM-3, a surface-to-bedrock record of the late Cenozoic sedimentation in Searles Valley, California: U.S. Geological Survey Professional Paper 1256, 24 p., https://doi.org/10.3133/pp1256.

Walker, J.D., and Andrew, J.E., 2019, Southern continuation and termination of the Airport Lake fault: Geological Society of America Annual Meeting, Abstracts with Programs, https://doi.org/10.1130/abs/2019AM-342036.

Walker, J.D., Black, R.A., Berry, A.K., Davis, P.J., Andrew, J.E., and Mitsdarfer, J.M., 2002, Geologic maps of the northern Mojave Desert and southwestern Basin and Range Province, in Glazner, A.F., Walker, J.D., and Bartley, J.M., eds., Geologic Evolution of the Mojave Desert and Southwestern Basin and Range: Geological Society of America Memoir 195, p. 295–296, 1:250,000.

Walker, J.D., Kirby, E., and Andrew, J.E., 2005, Strain transfer and partitioning between Panamint Valley, Searles Valley, and Ash Hill fault zones, California: Geosphere, v. 1, p. 111–118, https://doi.org/10.1130/GES00014.1.

Walker, J.D., Bigoli, T.S., Didericksen, B.D., Stockli, D.F., and Andrew, J.E., 2014, Middle Miocene to recent exhumation of the Slate Range, eastern California, and implications for the timing of extension and the transition to transtension: Geosphere, v. 10, no. 2, p. 276–291, https://doi.org/10.1130/GES00947.1.

Walker, J.D., Geissman, J.W., Bowring, S.A., and Babcock, L.E., compilers, 2018, Geologic Time Scale v. 5.0: Geological Society of America, https://doi.org/10.1130/2018.CTS005R3C.

Walker, J.D., Monastero, F.C., Andrew, J.E., Kirby, E., and Unruh, J.R., 2019, The M7.1 and 6.4 Ridgecrest earthquakes on the Airport Lake fault connect Owens Valley to the Garlock fault: Abstract #S34C-07 presented at 2019 Fall Meeting, AGU, San Francisco, California, 9–13 December.

Yeats, R.S., Cole, M.R., Merschat, W.R., and Parsley, R.M., 1974, Poway Fan and Submarine Cone and Rifting of the Inner Southern California Borderland: Geological Society of America Bulletin, v. 85, p. 293–302, https://doi.org/10.1130/0016-7606(1974)85<293:PFASCA>2.0.CO;2.

Zhang, P., Ellis, M., Slemmons, D.B., and Mao, F., 1990, Right-lateral displacements and the Holocene slip rate associated with prehistoric earthquakes along the southern Panamint Valley fault zone; implications for southern Basin and Range tectonics and coastal California deformation: Journal of Geophysical Research, v. 95, p. 4857–4872.